Non-adiabatic dissociation dynamics of Ar···I₂ (E, v) intermolecular vibrational levels probed using velocity-map imaging

Cite as: J. Chem. Phys. 159, 104305 (2023); doi: 10.1063/5.0166512 Submitted: 5 July 2023 • Accepted: 21 August 2023 • **Published Online: 8 September 2023**









Camille Makarem^{a)} (D) and Richard A. Loomis^{b)} (D)



AFFILIATIONS

Department of Chemistry and Institute of Materials Science and Engineering, Washington University in St. Louis, St. Louis, Missouri 63130, USA

- ^{a)}Present address: Laser Interferometer Gravitational-Wave Observatory (LIGO) Laboratory, California Institute of Technology, Pasadena, California 91125, USA.
- b) Author to whom correspondence should be addressed: loomis@wustl.edu

ABSTRACT

Ion time-of-flight velocity-map imaging was used to measure the kinetic-energy distributions of the I₂ ion-pair fragments formed after photo excitation of Ar $\cdot \cdot I_2$ complexes to intermolecular vibrational levels bound within the Ar + I_2 (E, $v_E = 0-2$) potential energy surfaces. The kinetic-energy distributions of the I_2 products indicate that complexes in the Ar $\cdot\cdot\cdot I_2$ (E, v_E) levels preferentially dissociate into I_2 in the D and β ion-pair states with no change in I₂ vibrational excitation. The energetics of the levels prepared suggest that there is a non-adiabatic coupling of the initially prepared levels with the continuum of states lying above the Ar + I₂ (D, $v_D = v_E$) and Ar + I₂ (β , $v_{\beta} = v_E$) dissociation limits. The angular anisotropies of the I₂ product signals collected for many of the Ar · · I₂ (E, v_E) levels have maxima parallel to the laser polarization axis. This contradicts expectations for the prompt dissociation of complexes with T-shaped geometries, which would result in images with maxima perpendicular to the polarization axis. These anisotropies suggest that there is a perturbation of the transition moment in these clusters or there are additional intermolecular interactions, likely those sampled while traversing above the attractive wells of the lower-energy potentials during dissociation. I₂ (D', v_{D'}) products are also identified when preparing several of the low-lying levels localized in the T-shaped well of the Ar + I_2 (E, $v_E = 0-2$) potentials, and they are formed in multiple $v_{D'}$ vibrational levels spanning energy ranges up to 500 cm⁻¹

Published under an exclusive license by AIP Publishing. https://doi.org/10.1063/5.0166512

I. INTRODUCTION AND BACKGROUND

The Ar \cdots I₂ van der Waals complex has proven to be a model system for investigating the dynamics and energy-transfer processes incurred after photoexcitation of weakly bound van der Waals complexes. $^{1-11}$ The Ar \cdots I₂ complexes prepared in intermolecular vibrational levels bound within the Ar + I_2 (B ${}^3\Pi_{0u}^+$, v_B) potential energy surfaces (PESs) may experience a variety of relaxation and dissociation processes, including vibrational predissociation (VP), intramolecular energy vibrational redistribution (IVR), and electronic predissociation.7-Transitions of the linear Ar \cdots I₂ $(X^1\Sigma_0^+, v_X = 0)$ conformer also access the repulsive, inner walls of the Ar + I2 (B, vB) intermolecular PESs lying energetically above each dissociation limit and undergo prompt dissociation. ^{10,1}

resultant continuum fluorescence of the I₂ (B, v_B) products is sometimes incorrectly associated with one-atom caging.

Far less is known about the dynamics of Ar···I₂ complexes photo excited to levels bound within the PESs associated with the ionpair states of I₂. As there are numerous first-tier ion-pair states with approximately the same vibrational frequencies, including the energetically nested I_2 (E 0_g^+), I_2 (D 0_u^+), I_2 (β 1_g), and I_2 (D' 2_g) states, the densities of states in this energy region are significantly higher and additional relaxation pathways exist. Two-color, two-photon laser-induced fluorescence (LIF) experiments have determined the binding energy of the Ar + I_2 (E, $v_E = 0-3$) PESs to be ~410 cm⁻¹ with a minimum in the T-shaped geometry. 24-26 We recently made assignments of the two-photon LIF features, and these indicate that levels with well-defined intermolecular bending and stretching excitation, n_b and n_s , can be accessed in the Ar + I_2 (E, v_E = 0–3) PESs. 24 Theoretical results obtained using diatomics-in-molecule with first-order perturbation (IDIM PT1) methods indicate that the Ar + I_2 (E, v_E) PESs and the potentials of most of the first-tier ion-pair states, including the Ar + I_2 (D, v_D) and Ar + I_2 (β , v_β) PESs, have overall minima in the T-shaped geometry. 27,28 The Ar + I_2 (D', v_D ') PES is the only first-tier ion-pair state system that has a minimum predicted to be in the linear geometry. 27

In this article, we report on the nonadiabatic dissociation dynamics of $Ar\cdots I_2$ complexes prepared in numerous intermolecular vibrational levels bound within the $Ar+I_2$ (E, $v_E=0$ –2) ion-pair state PESs, which are identified using the $(n_b, n_s)_{vE}$ notation. ²⁴ The spectroscopic results ²⁴ combined with calculations of the wavefunctions of the $Ar\cdots I_2$ levels bound within the $Ar+I_2$ (B, v_B) potentials indicate that all of the $(n_b, n_s)_{vE}$ levels accessed are localized in the T-shaped region of the intermolecular PES. The lowest-energy $(0,0)_{vE}$ levels sample approximately $\pm 10^\circ$ from 90° and are considered to have rigid T-shaped geometries. Even the levels of slightly higher energies are quite localized in the T-shaped wells, lying well below the barrier for rotation of the Ar atom about the I_2 moiety.

A major hypothesis at the onset of these experiments was that the nonadiabatic dynamics experienced by the I_2 (E, $v_E = 0{\text -}2$) moieties within $Ar \cdots I_2$ complexes during dissociation would contrast those identified in the $Ar + I_2$ (E, $v_E = 0{\text -}2$) collisional studies reported on previously²⁹ since the inner repulsive wall region of the PESs that dominates during full-collision events is not directly accessed by the complexes. Furthermore, the energetics of the full-and half-collision events are notably different. The full-collisions occur with thermal distributions of translational energies above the asymptotes of the $Ar + I_2$ (E, $v_E = 0{\text -}2$) PESs and from all intermolecular orientations. In contrast, the dissociation in the half-collision events are initiated from preferred orientations dictated by the intermolecular vibrational wavefunctions of the $(n_b, n_s)_{vE}$ levels prepared and with discrete energies, lying 300–400 cm⁻¹ below each $Ar + I_2$ (E, $v_E = 0{\text -}2$) dissociation limit.

We chose to investigate the dissociation dynamics of the $Ar\cdots I_2$ $(n_b,\ n_s)_{vE}$ levels with no or little I_2 vibrational excitation, $v_E=0-2$, to limit the densities of states of other intermolecular levels that may couple to the initially prepared levels and the number of energetically open product channels that may be formed. The mechanism of IVR alone is not open for the lowest-energy levels within the $Ar+I_2$ $(E,v_E=0)$ PES, but there are intermolecular levels associated with other ion-pair states in this energy region.

Ion time-of-flight velocity-map imaging (VMI) 22,30,31 was implemented to measure the momentum and, thus, the kinetic-energy distributions of the I_2 products formed in several different ion-pair states following these half-collision dissociation events. The anisotropies of the features within each ion image collected were characterized to provide additional insights into the dissociation pathways. We compare the VMI results with recent, half-collision $Ar \cdots I_2$ dissociation dynamics investigations of Baturo *et al.*, who probed the dissociation of intermolecular vibrational levels within the $Ar + I_2$ (E, $v_E = 2-5$) PESs, and with the results obtained from $Ar + I_2$ (E, $v_E = 0-2$) full-collision studies undertaken by Tscherbul *et al.* 29

II. EXPERIMENTAL DETAILS AND METHODS

Ground-state linear and T-shaped Ar \cdots I₂ (X, v_X = 0) complexes were stabilized in a pulsed, supersonic expansion, as previ-4,30 Experiments were performed using a gas ously described.^{6,7,22,2} mixture comprised of 10% Ar in He and a backing pressure of ~7000 Torr that was passed over room-temperature iodine crystals and pulsed into vacuum. The ion time-of-flight VMI experiments were performed in a similar manner as previously described. 7,22,5 supersonic expansion entered the ionization region of the chamber through a 2 mm skimmer and continued along a collinear electrostatic-lens assembly comprised of three electrode disks: a repeller (2158 V), an extractor (1500 V), and a ground electrode. Pulses from two nanosecond dye lasers were counter propagated on an axis orthogonally intersecting the 15 Hz pulsed molecular beam midway between the repeller and extractor electrodes. The wavenumber of the excitation laser, E_1 , was fixed on the rotational bandhead of the T-shaped Ar \cdots I₂ transition in the I₂ B-X, 23-0 spectral region, $E_1 = 18169.57$ cm⁻¹, thereby promoting Ar···I₂ complexes to the n' = 0 lowest-energy intermolecular vibrational level within the Ar + I_2 (B, $v_B = 23$) PES. The pulse fluence of the E_1 laser was 6–30 mJ cm⁻² in the interaction region. The wavenumber of the second laser, E_2 , was fixed on a transition from the metastable, T-shaped Ar $\cdot \cdot \cdot I_2$ (B, $v_B = 23$, n' = 0) level to an $(n_b, n_s)_{vE}$ intermolecular level with $v_E = 0-2$, which were reported recently.²⁴ The pulse fluence of the E_2 laser was >60 mJ cm⁻² so that I_2 ion-pair state products formed by the dissociation of the Ar···I₂ (E, $v_E = 0-2$) complexes could be ionized via non-resonant absorption of two additional E_2 photons. The timing of the two lasers was fixed so that the pulses spatially overlapped in the ionization region. In separate experiments performed to identify contributions in the VMI data from background signals and I₂ (B, v_B) products, the E_2 laser was delayed by ~15 ns from the E_1 laser.

The electrostatic lenses directed the ${\rm I_2}^+$ cations associated with the ${\rm I_2}$ dissociation products down a 1.57 m field-free flight tube onto a position-sensitive microchannel plate (MCP) detector with a phosphor screen. The MCP was time-gated for arrival of the ${\rm I_2}^+$ cations. The polarization axes of the two lasers were oriented parallel to the MCP detector face along the vertical direction, $\theta=0^\circ$. An ion image was acquired for each laser pulse using a charge-coupled device camera with only one to two ${\rm I_2}^+$ cations detected per pulse; images collected with higher cation counts were found to be slightly distorted in angular regions with the highest ion counts. Accumulated images were typically obtained by summing over 200 000–500 000 individual images.

Additional VMI experiments were performed using the outputs of three dye lasers so that the photon energy of the ionization laser could be varied independently from the energies of the Ar··I₂ B–X, 23–0 and E–B, v_E –23 excitation lasers. In addition, the timing of the ionization laser in this scheme could be delayed from the two-color, two-photon excitation. These experiments also helped in identifying the ion-pair states contributing to the VMI data based on one- and two-photon ionization selection rules. In these experiments, the wavenumber of the excitation laser pulse, E_1 , was fixed on the transition of the T-shaped Ar··I₂ complex to the lowest-energy intermolecular vibrational level, n'=0, in the I₂ B–X, 23–0 spectral region. The wavenumber of the second laser, E_2 , was fixed on

an Ar···I₂ E-B, v_E-23 transition from the intermediate T-shaped, n' = 0 level to an $(n_b, n_s)_{vE}$ intermolecular level with known quanta of n_b and n_s. The I₂ products in the ion-pair states were ionized with the frequency-doubled output of a third dye laser. The wavenumber of the ionization laser, E_3 , was fixed on a value in the range $33\,960-34\,400\,\mathrm{cm}^{-1}$, thus promoting the I₂ ion-pair fragments above the ionization potential, 75 069 cm⁻¹. The E_1 and E_2 laser pulses were co-propagated and overlapped in time, and the E_3 pulses were counter propagated to the E_1 and E_2 laser pulses. The E_3 pulses were normally overlapped in time with the E_1 and E_2 pulses. The three lasers were vertically polarized in a direction perpendicular to the face of the MCP detector. The I2+ images were acquired and accumulated in the same manner as in the two-laser VMI experiments with only one to two I_2^+ cations detected per pulse. The pulse fluence of the second laser was decreased, <1.0 mJ cm⁻², to minimize the ionization of I_2 products by E_2 photons. Negligible cations were detected when either the E_1 or E_2 lasers were blocked in these three-color experiments.

III. RESULTS

A. I₂ product channels

Kinetic-energy release distributions. Ion time-of-flight VMI was used to measure the momentum and kinetic-energy distributions of the I2 ion-pair state fragments formed by the dissociation of numerous $Ar \cdot \cdot \cdot I_2$ $(n_b, n_s)_{vE}$ levels. The n' = 0 level in the Ar + I_2 (B, v_B = 23) PES with a rigid T-shaped geometry was used as the intermediate level, $E_1 = 18169.57$ cm⁻¹, and E_2 was fixed on Ar $\cdot \cdot \cdot I_2$ transitions in the I_2 E-B, ν_E -23 region to specific $(n_b, n_s)_{vE}$ levels that are not overlapped by other $Ar \cdot \cdot \cdot I_2$ transitions.²⁴ The I₂ product momentum distributions were obtained using the BASEX program³³ to perform inverse Abel transforms of the I_2^+ images collected for each E_2 and integrating over the angular coordinate, θ , where $\theta = 0^{\circ}$ is the laser polarization axis. The momentum resolution of the I2 fragments was measured to be <3% of the momentum. The kinetic-energy distributions of the I_2 products, $KE(I_2)$, were calculated from the calibrated momentum distributions. The kinetic-energy release, KER, distributions of the Ar and I₂ dissociation fragments were obtained using conservation of momentum, KER = $(m_{Ar} \cdot \cdot \cdot_{I2}/m_{Ar}) \cdot \text{KE}(I_2)$, where $m_{Ar} \cdot \cdot \cdot_{I2}$ and m_{Ar} are the masses of the Ar···I₂ complex and the Ar atom.

The KER distributions resulting from the dissociation of complexes prepared in 14 different $(n_b,\,n_s)_{vE}$ intermolecular vibrational levels within the Ar + I_2 (E, v_E = 0–2) PESs were measured. Six of the KER distributions are plotted in Fig. 1, and the KER distributions for all 14 levels are included in supplementary material. The KER distributions obtained when exciting some of the levels, e.g., the rigid T-shaped $(0,\,0)_0$ level and the $(2,\,1)_0$ level with both intermolecular bending and stretching excitation, are weak with non-descript structures that extend over broad energy regions. Other distributions, such as measured for excitation of the $(0,\,1)_0$ level, have a single, broad peak. The KER distributions obtained for most of the levels, e.g., the $(2,\,0)_0,\,(2,\,0)_1,\,$ and $(0,\,3)_1$ levels, have higher product ion counts and multiple discernible product peaks.

Three-laser VMI experiments were performed to verify that the ${\rm I_2}^+$ cations detected were associated with the dissociation of ${\rm Ar} \cdots {\rm I_2}$ (E, ${\rm v_E}$) complexes in the prepared $(n_b, \, n_s)_{vE}$ intermolecular vibrational levels and not with the dissociation of metastable

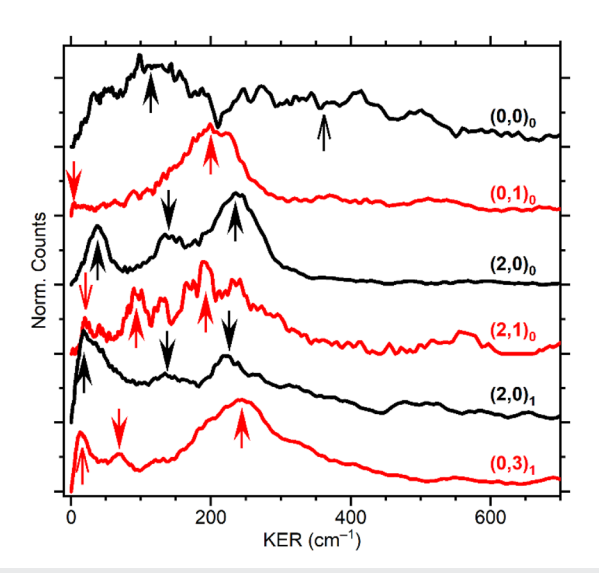


FIG. 1. Kinetic-energy release (KER) distributions measured using $E_1 = 18169.57$ cm⁻¹ and E_2 fixed on transitions to the intermolecular vibrational levels²⁴ indicated on the right. The bottom axis represents the total KER. The anisotropy plots of the ion images measured at the filled arrows are included in Fig. 5. All of the anisotropy plots, including those measured at the energies of the open arrows, are included in the supplementary material.

ionized complexes bound within Ar + $I_2^+(X, v_X)$ PESs. Two-color, two-photon excitation with wavenumbers E_1 and E_2 were used to prepare the complexes in $(n_b, n_s)_{vE}$ levels with $v_E = 0$ and 1 in the same manner as described above. A third, separately tunable laser, with wavenumber E_3 , was used for one-color ionization from the I₂ ion-pair states. The laser pulses from all three lasers were overlapped in time in order to enable metastable complexes prepared in the $(n_b, n_s)_{vE}$ levels to be ionized to $Ar \cdot I_2^+(X, v_X)$ complexes. These ionized complexes would likely dissociate into Ar + $I_2^+(X, v_X)$ fragments with a total KER that would depend on the wavenumbers of E_3 . This was not observed; the maximum kinetic energies of the I_2^+ fragments did not change with E_3 . The relative intensities of the peaks within the KER and KE(I2) distributions did vary with E₃ due to changing Franck-Condon factors in the ionization step. Since the lifetimes of the I2 molecules in the ion-pair states are comparable to the durations of the laser pulses, the E_3 pulses could not be delayed from the E_1 and E_2 pulses to differentiate between further excitation of the Ar...I2 (E, vE) complexes and I2 products. Nevertheless, there is no evidence for contributions from ionized complexes in the VMI images, and the dissociation dynamics interrogated in the VMI experiments are associated with the $Ar \cdot \cdot \cdot I_2$ (E, v_E) complexes.

Product-channel assignments. Each of the KER distributions recorded using $E_1 = 18169.57~{\rm cm}^{-1}$ and E_2 fixed on specific ${\rm Ar} \cdot \cdot \cdot {\rm I}_2$ transitions in the ${\rm I}_2$ E-B, ${\rm v}_E$ -23 region was fit to a sum of Lorentzian peak functions to approximate the center energies and breadths of the discernible peaks within each distribution. The momentum distributions, the kinetic-energy distributions plotted as a function of KER, and the Lorentzian fits of the peaks are included in the supplementary material. The energies of the peaks and qualitative descriptors of the relative intensities of the peaks are listed in

Tables SI and SII in the supplementary material. The VMI data and KER distributions for several $(n_b, n_s)_{vE}$ levels could not be collected due to spectral congestion, overlapping transitions, and extremely weak ion signals. Some of the background counts and noise in the KER distributions were from the presence of I_2^+ background counts formed by non-resonant multiphoton ionization with the E_2 laser. The amounts of these background counts were independent of the E_2 photon wavenumber and were observed without the presence of the E_1 excitation pulses (see example data in Fig. S5 of the supplementary material).

The results of the KER peak fitting and the I_2 energy-level diagrams in Fig. 2 provide insights into the $Ar+I_2$ product channels formed after excitation to the different $(n_b,\ n_s)_{vE}$ intermolecular vibrational levels, which are indicated as short black, horizontal lines. The vertical axes in Fig. 2 represent the energies below each of the $Ar+I_2$ (E, $v_E=0$ –2) dissociation limits. For example, the lowest-energy $(0,0)_0$ level, on the left in Fig. 2(a), is at 410.3 cm $^{-1}$, which

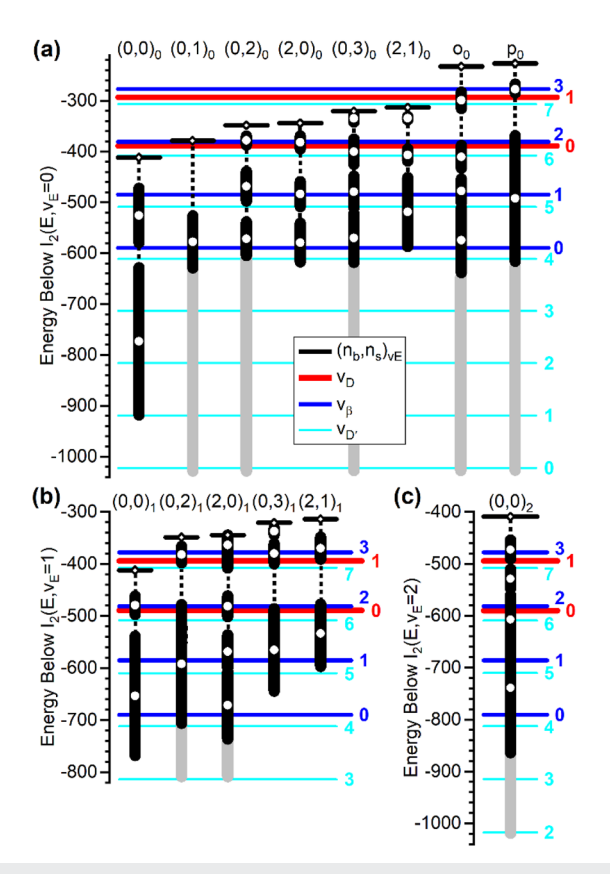


FIG. 2. Energetics of Ar···l₂ (E, v_E) levels prepared and I₂ products identified. (a)–(c) include the $(n_b,\,n_s)_{vE}$ intermolecular levels bound within the Ar + I₂ (E, v_E = 0–2) PESs that were photoexcited (black horizontal lines). The o₀ and p₀ labels are included in (a) since these transitions were not assigned. The energy scales are relative to the Ar + I₂ (E, v_E = 0–2) dissociation limits. The energies of the I₂ vibrational levels of the D,³⁴ β ,³⁵ and D'³⁶ ion-pair states are indicated by red, blue, and cyan lines, respectively. White circles and black vertical bars are the energies and breadths of the peaks in the KER distributions. A few KER distributions contain a broad tail extending beyond the features (gray vertical bars).

is the binding energy, $D_0(E)$, of the Ar + I₂ (E, v_E = 0) PES.²⁴ The energies of the molecular vibrational levels of the I₂ (D),³⁴ I₂ (β),³⁵ and I₂ (D')³⁶ states are indicated as red, blue, and cyan horizontal lines, respectively. The center energies and breadths (full-width at half maximum) of the peaks identified in the KER distributions are indicated as white circles and black vertical bars in Fig. 2. Several of the KER distributions contain a tail extending to higher KER values, and these tails are represented by gray vertical bars. As mentioned, the I₂⁺ counts were particularly low when collecting the VMI data for several of the (n_b, n_s)_{vE} levels, and assignment of peaks in these KER distributions was difficult. For these distributions, numerous ion images were recorded, and only those peaks that were discernible in all datasets were fit and included (see Fig. S6 of the supplementary material).

The KER distributions measured when promoting Ar···I2 complexes to the $(0, 2)_0$, $(2, 0)_0$, $(0, 3)_0$, and $(2, 1)_0$ levels as well as those measured with excitation of the oo and po transitions, for which assignments of intermolecular bending and stretching excitation were not made,²⁴ each have multiple peaks, Fig. 2(a). The peak with the highest-KER in each of these distributions, or the largest amount of energy below the I_2 (E, $v_E = 0$) level, has the highest intensity. These peaks overlap the energies of the I_2 (β , $v_\beta = 0$) or I_2 $(D', v_{D'} = 4)$ states. The KER distribution for each of these five levels has a weaker peak at lower energies that overlaps the energies of the I_2 (D, v_D = 0), I_2 (β , v_{β} = 2), and I_2 (D', $v_{D'}$ = 6) states. When promoting the Ar·· I_2 complexes to the $(0, 2)_1$, $(2, 0)_1$, $(0, 3)_1$, and (2, 1)₁ intermolecular vibrational levels, the highest-KER peak in each distribution overlaps the energies of the I_2 (β , $v_\beta = 1$) and I_2 (D', $v_{D^{\prime}}$ = 5) states. The lowest-energy peak in each distribution spans the energies of the I_2 (D, $v_D = 1$), I_2 (β , $v_{\beta} = 3$), and I_2 (D', $v_{D'} = 7$) vibrational states.

Preliminary assignments of the peaks in the KER distributions to specific I2 ion-pair states were made based on the assumption that no change in I2 vibrational excitation occurred throughout the dissociation. This assumption suggests that the peaks observed at highest KER in the distributions recorded after preparing the $(n_b, n_s)_0$ levels, those with I_2 (E, $v_E = 0$), are associated with the Ar + I_2 (β , v_β = 0) product channel. Similarly, the lower-energy peaks are associated with the Ar + I₂ (D, v_D = 0) products. The higherenergy peaks in the KER distributions recorded after exciting to the $(n_b,\,n_s)_1$ levels are associated with the Ar + I_2 $(\beta,\,v_\beta$ = 1) product channel, and the lower-energy peaks are attributed to the Ar + I2 (D, $v_D = 1$) channel. The peaks associated with the $\Delta v = 0$, Ar + I₂ (β , v_{β}) product channels have larger counts than those attributed to the $\Delta v = 0$, Ar + I₂ (D, $v_D = 1$) products in all of these KER distributions. See the insets in Figs. S1-S4 in the supplementary material for the fitted areas of the Lorentzian peaks.

The KER distributions measured for excitation of the rigid T-shaped levels $(0, 0)_0$, $(0, 0)_1$, and $(0, 0)_2$ are different than most of the other distributions. For these excitations, the Ar + I₂ (D, v_D) product asymptotes that maintain I₂ vibrational excitation, v_D = v_E, are not energetically accessible. The highest-energy peaks are broader than most of the peaks in the other distributions, and they have tails extending beyond the energies of the Ar + I₂ (β , v_{β}) Δ v = 0 channels. The high-energy tails present in some of the KER distributions (gray bars in Fig. 2) are associated with dissociation into the Ar + I₂ (D', v_{D'}) products. The large breadths of these sig-

nals and the lack of peaks within them suggest that the I_2 (D', $v_{D'}$) products are likely rotationally hot.

The KER distributions presented thus far were collected using $E_1=18169.57~{\rm cm}^{-1}$ to prepare the T-shaped n' = 0 level in the Ar + I₂ (B, v_B = 23) PES as the intermediate and E_2 to access the (n_b, n_s)_{vE} intermolecular vibrational levels bound within the Ar··I₂ (E, v_E = 0–2) and ionize the I₂ dissociation products. This two-photon, non-resonant ionization from the I₂ ion-pair states creates ions in high-lying vibrational levels in either the I₂+(X²Π_{3/2}) or I₂+(X²Π_{1/2}) ion states. Due to the conservation of angular momentum, this ionization results in preferential detection of products in vibrational levels of the I₂ (β I_g) ion-pair state, and the probability for ionizing molecules in the I₂ (D' 2_g) and I₂ (D 0_u⁺) states is lower.

In order to differentiate the contributions of products in the different ion-pair states, additional VMI experiments were performed using three lasers. The E_1 and E_2 lasers were fixed on the same wavenumbers, and much lower fluences were used for E_2 so that negligible ions were detected with both lasers present and overlapped in time. A third laser with $E_3 = 344\,60.0\,\mathrm{cm}^{-1}$ was overlapped in time with the E_1 and E_2 lasers. This photon energy is sufficient for single-photon ionization from the ion-pair states, and the relative transition strengths are reversed; the probabilities for single-photon ionization from the I_2 (D' I_2) and I_3 (D I_2 0 I_3 1 states are higher than from the I_3 2 (B I_3 1 ion-pair state.

The KER distribution obtained using three colors (one-photon ionization) and accessing the $(2,0)_0$ level within the Ar + I₂ (E, $v_E = 0$) PES is plotted as gray in Fig. 3. The KER distribution obtained using two colors (two-photon ionization) and accessing the same $(2,0)_0$ level is plotted as black. Each distribution contains three discernible peaks, near 38, 140, and 235 cm⁻¹. The peak at 235 cm⁻¹ overlaps the energies of the I₂ (β , $v_{\beta} = 0$) and I₂ (D', $v_{D'} = 4$)

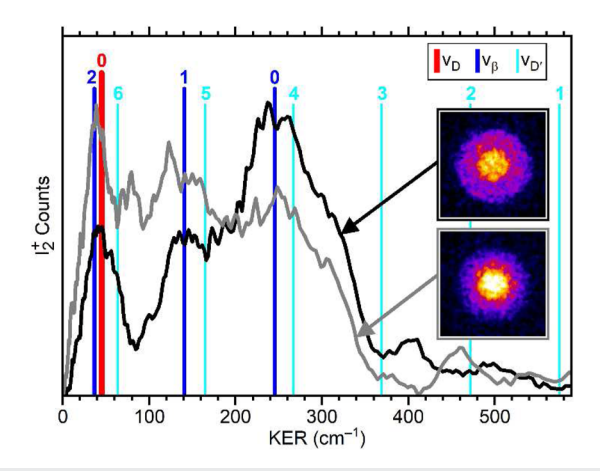


FIG. 3. KER distributions measured following excitation to the $(2, 0)_0 \text{ Ar} \cdot \cdot \cdot l_2$ (E, $v_E = 0$) level. The black distribution was acquired in two-laser experiments via a two-photon ionization process, $E_2 = 230\,83.4\ \text{cm}^{-1}$. The gray distribution was collected in three-laser experiments via a one-photon ionization process. The l_2^+ ion images associated with each distribution are included. The red, blue, and cyan vertical lines represent the l_2 vibrational energy levels of the D, 34 β , 35 and D' 36 states

levels. Since this peak is more pronounced in the two-photon ionization distribution (black), this peak is primarily associated with the Ar + I_2 (β , v_{β} = 0) product channel. The peak centered at 38 cm⁻¹ overlaps the energies of the I_2 (β , v_{β} = 2), I_2 (D, v_D = 0), and I_2 (D', $v_{D'}$ = 6) levels. Since ionization to the I_2 (β , v_{β} = 2) level should be weaker in the single-photon ionization KER distribution (gray), this peak is primarily attributed to the $\Delta v = 0$, I₂ (D, $v_D = 0$) products. Note that the counts of the Ar + I₂ (β , $v_{\beta} = 0$) peak are less than the Ar + I_2 (D, $v_D = 0$) peak in the KER distribution obtained using one-photon ionization, gray in Fig. 3, while the peak intensities are the opposite in the two-photon ionization KER distribution (black). Accurate comparisons of the relative yields for the formation of these products are not made as quantitative transition strengths for the one- and two-photon ionization transitions are not known. There may also be contributions from I_2 (D', $v_{D'} = 6$) products overlapping the I₂ (D, v_D = 0) signals. The intensity of the KER peak at 140 cm⁻¹, which overlaps the I_2 (β , v_{β} = 1) and I_2 (D', $v_{D'}$ = 5) levels, is higher in the one-photon KER distribution than in the two-photon distribution. This peak and the other ion signals spanning the entire breadth of the distribution are associated with non-adiabatic coupling and dissociation to the Ar + I_2 (D', $v_{D'}$)

Probing coupling mechanisms. The KER distributions measured when exciting the $(2, 0)_0$ and $(0, 2)_0$ levels, which are within 5 cm⁻¹ of each other, are plotted in Fig. 4 as black and gray. These data were collected using two colors, one for initial excitation and one for secondary excitation to the $(v_b, v_s)_{vE}$ level and two-photon ionization. The dominant peak in each distribution is the highenergy peak, at ~230 cm⁻¹, which is associated with the Ar + I₂ $(\beta, v_\beta = 0)$ channel. The relative intensities of the peak at 230 cm⁻¹ to the lowest-energy peak in each distribution, which is associated with the Ar + I₂ $(D, v_D = 0)$ channel, are significantly different in these distributions. These product yields could be associated with a dependence of coupling on the intermolecular vibrational excitation or the regions of the multi-dimensional PES sampled. There

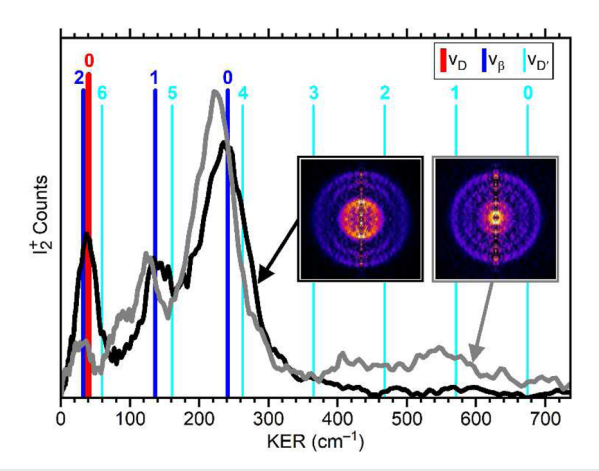


FIG. 4. KER distributions measured following excitation to the (2, 0)₀, $E_2 = 230\,83.4\,\mathrm{cm}^{-1}$, and (0, 2)₀, $E_2 = 230\,78.8\,\mathrm{cm}^{-1}$, intermolecular levels, black and gray, respectively. The inverse-Abel transformed ion image associated with each distribution is included. The red, blue, and cyan vertical lines represent the energies of the I₂ vibrational levels of the D, $^{34}\,\beta$, 35 and D' 36 states.

could be a propensity for coupling to Ar + I_2 (D, v_D) channels for $(n_b,\,n_s)_{vE}$ intermolecular vibrational levels with bending excitation, $n_b>0$, that would sample geometries away from the T-shaped geometry. Those levels that remain localized in the T-shaped well or only have intermolecular stretching excitation could preferentially couple with the Ar + I_2 (β,v_β) channels. In contrast, there could be energetic resonances of the $(n_b,\,n_s)_{vE}$ levels with optically dark levels associated with the PESs associated with the other ion-pair states accessed during dissociation are very narrow, $<5~cm^{-1}$.

The KER distributions indicate that the coupling of the prepared $(n_b,v_s)_{vE}$ levels to the Ar + I_2 (D', $v_{D'}$) channels cannot be solely dictated by the specific intermolecular vibrational excitation of that level. The KER distribution measured for the $(2,\,0)_1$ level contains a reproducible I_2 product tail extending to higher KER value that is associated with Ar + I_2 (D', $v_{D'}$ = 0–3) products. In contrast, there is no to tail and, thus, no evidence for forming Ar + I_2 (D', $v_{D'}$) products when exciting the $(2,\,0)_0$ level. These results are switched for excitation of the $(0,\,3)_1$ and $(0,\,3)_0$ levels with coupling to the Ar + I_2 (D', $v_{D'}$) products observed for the level bound within the Ar + I_2 (E, v_E = 0) potential, but not within the Ar + I_2 (E, v_E = 1) potential.

B. Product-channel anisotropies

Expectations and limits. The angular distributions of the peaks in the VMI images were analyzed to identify possible correlations between the (n_b, n_s)_{vE} intermolecular vibrational levels prepared and the I2 product channels assigned in order to gleam information about the dissociation mechanisms and pathways. A similar methodology was used to verify the role of IVR during the dissociation of T-shaped Ar···I2 complexes prepared in the lowest-energy levels bound within the Ar + I_2 (B, v_B) PESs.⁷ The vibronic excitation in the I2 B-X region is a parallel transition, and the Ar atom in the complex should not significantly alter this. As a result, vertical polarization of the excitation laser, defined as $\theta = 0^{\circ}$, will preferentially excite rigid T-shaped Ar \cdots I₂ complexes with the intermolecular axis lying in the horizontal plane. The prompt dissociation from this distribution of initial orientations would result in Ar and I2 fragments having kinetic energies preferentially along θ = 90°, forming an $I(\theta)$ $\propto \sin^2 \theta$ distribution. Angular distributions of the I₂ (B, v < v_B) products with maxima not along the horizontal $\theta = 90^{\circ}$ direction were attributed to IVR to levels with intermolecular bending excitation prior to dissociation.7

The dissociation dynamics experiments reported here were performed using a two-color, two-photon excitation scheme with $E_1 = 181\ 69.57\ \text{cm}^{-1}$, thereby accessing the lowest-energy, T-shaped level in the $I_2\ B-X$, 23-0 region, and $E_2\ fixed$ on $Ar\cdots I_2$ transitions in the $I_2\ E-B$, v_E-23 spectral region to prepare the complexes in specific $(n_b,n_s)_{vE}$ levels. Both of these are parallel transitions for molecular $I_2.^{37,38}$ The transition moment of the complex should also lie predominantly along the I–I bond axis in the limit that any mixing of the initially prepared $Ar\cdots I_2\ (E,v_E)$ states with the other ion-pair states, and the presence of the Ar atom does not significantly alter the orientation of the I_2 transition moment. With these assumptions, the I–I bond axis in the $Ar\cdots I_2\ (E,v_E)$ complexes excited would be oriented with a $\cos^4\theta$ distribution about the vertical polarization axis, $\theta=0^\circ$. The prompt dissociation of rigid T-shaped complexes from this distribution of initial orientations would result in Ar and I_2

fragments having kinetic energies preferentially along $\theta=90^\circ$ with an $I(\theta) \propto \sin^4 \theta$ distribution. Dissociation of complexes with non-rigid geometries, such as those in $Ar \cdot \cdot \cdot I_2$ (E, v_E) levels with bending excitation, would likely result in deviations away from this distribution. Long-lived states or those with the Ar atom fully delocalized in the angular coordinate about the I_2 moiety would result in isotropic distributions. The non-adiabatic coupling of the $Ar \cdot \cdot \cdot I_2$ (E, v_E) levels to excited $Ar \cdot \cdot \cdot I_2$ levels within the PESs of the other ion-pair states could also result in products not having a $\sin^4 \theta$ distribution.

Inverse Abel transformations of the VMI images were used to obtain the angular distributions of the $\rm I_2$ ion-pair state products at the peak energies identified within the KER distributions. For a prompt two-body photodissociation process induced via two-photon absorption, the angular distribution of the fragments is expressed by 32,39,40

$$I(\theta) = \frac{1}{4\pi} \left[1 + \beta_2 P_2(\cos \theta) + \beta_4 P_4(\cos \theta) \right]. \tag{1}$$

The angle between the polarization axis of the lasers and the fragment recoil vector is θ , and $P_2(\cos \theta) = (3\cos^2 \theta - 1)/2$ and $P_4(\cos \theta)$ θ) = $(35\cos^4\theta - 30\cos^2\theta + 3)/8$ are the second and fourth Legendre polynomials, respectively. As mentioned, for the limiting case of the dissociation of rigid T-shaped complexes, the I₂ molecules would recoil in a direction perpendicular to the laser-polarization axis, and the product distribution would be $I(\theta) \propto \sin^4 \theta$. The anisotropy parameters for this scenario would be $\beta_2 = -1.43$ and $\beta_4 = +0.43$, 32 which are abbreviated as $[\beta_2/\beta_4] = [-1.43/+0.43]$. In contrast, the two-photon excitation and prompt dissociation of a complex with a linear I-I···Ar geometry would generate I2 fragments recoiling along the laser-polarization axis, and a fragment distribution of $I(\theta) \propto \cos^4 \theta$ and anisotropy parameters of [+2.86/+1.14] would result. If there were strong coupling between ion-pair states, a twophoton excitation with one parallel and one perpendicular transition could result, and the distribution would be $I(\theta) \propto \cos^2 \theta \sin^2 \theta$ with maxima at $\theta = 45^{\circ}$ and 135° and anisotropy parameters of [+0.71/-1.71]. These different I₂ angular distributions would be expected for the dissociation of complexes with rigid geometries, but variations between these limits are likely when the complexes are promoted to levels with intermolecular bending and stretching excitation.

The angular distribution for many of the peaks identified in the KER distributions obtained when exciting the different (n_b, n_s)_{vE} intermolecular vibrational levels, including those indicated by arrows in Fig. 1, and their fits to Eq. (1) are included in the supplementary material. The β_2 and β_4 anisotropy parameters obtained by fitting the angular anisotropy plot for each peak to Eq. (1) are included in Tables SI and SII in the supplementary material. The weak signal levels in some of these distributions and the presence of background signals, which add an offset of ion counts to the anisotropy plots, made quantitative determination of the anisotropy parameters for some peaks particularly difficult. Most of the angular distributions have identifiable maxima, but none of the pairs of anisotropy parameters are particularly close to the limits associated with $\cos^4 \theta$, $\sin^4 \theta$, or $\cos^2 \bar{\theta} \sin^2 \theta$ product distributions and the prompt dissociation of rigid T-shaped or linear complexes. Angular distributions with fitted β_2 and β_4 parameters both within three times the uncertainty from zero were identified as isotropic.

T-shaped levels. The lowest-energy intermolecular vibrational level bound within the Ar + I₂ (E, $v_E = 0$) PES is the rigid T-shaped (0, 0)₀ level, and it lies energetically just below the asymptotes for forming I₂ (D, $v_D = 0$), I₂ (β , $v_\beta = 2$), and I₂ (D', $v_{D'} = 6$) products, as indicated in Fig. 2(a). The KER distribution measured when preparing this T-shaped level has two weak peaks, one at ~114 cm⁻¹ and a

second at ~352 cm⁻¹. The angular distribution of the 114 cm⁻¹ peak, first column in Fig. 5(a), is slightly anisotropic with maxima near $\theta=45^{\circ}$ and 135° and anisotropy parameters of [+0.21(4)/–0.30(5)]. As this maximum in the KER distribution is more than 60 cm⁻¹ above the Ar + I₂ (β , v $_{\beta}=0$) asymptote, this peak is associated with a distribution of I₂ rotational states, which would lead to a more

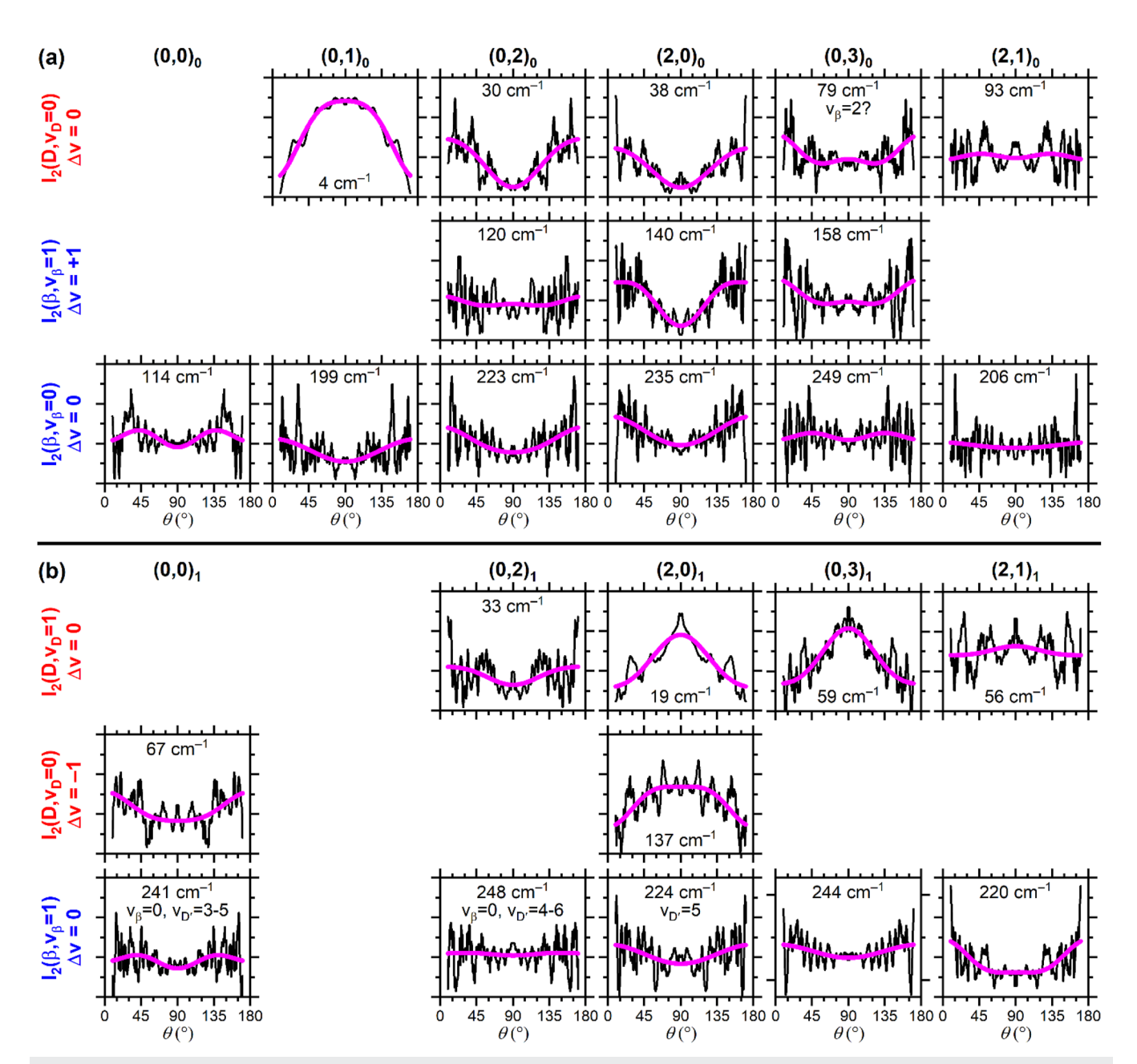


FIG. 5. Anisotropy plots (black) and fits (magenta) of the peaks in the I_2^+ images. Plots obtained with excitation of the $(n_b, n_s)_0$ levels are in (a) and the $(n_b, n_s)_1$ levels are in (b) with the specific levels prepared indicated at the top of each column. The kinetic-energy release of the peak associated with each plot is included. The polarization axes of E_1 and E_2 are along $\theta = 0^\circ/180^\circ$. The prominent I_2 product channel proposed for each peak is indicated at the left. A few of the high-energy distributions for the $(n_b, n_s)_1$ levels may contain contributions from other product channels and those are indicated.

isotropic angular distribution. Furthermore, there may also be contributions from I_2 (D', $v_{D'}=4,5$) products that energetically overlap the I_2 ($\beta,\,v_\beta=0$) products. The peak centered at ~352 cm $^{-1}$ spans a broad range of energies, ~290 cm $^{-1}$, and it overlaps the energies of the I_2 (D', $v_{D'}=1{\text -}3$) products. The angular distribution for this peak is considered isotropic with [+0.2(1)/0.0(1)] (Fig. S7 in the supplementary material).

The angular distributions measured when exciting the T-shaped (0, 0)₁ level with one quantum of I₂ molecular vibrational excitation are slightly different than those for the $(0, 0)_0$ level. The KER distribution for the (0, 0)1 level has two prominent peaks at ~67 and ~241 cm⁻¹. The $\Delta v = 0$ channel for formation of Ar + I₂ (D, v_D = 1) products is also not energetically open for this excitation. The low-energy peak at 67 cm⁻¹ is centered just 10 cm⁻¹ above the $\Delta v = -1$, Ar + I₂ (D, $v_D = 0$) asymptote and is fairly narrow, ~35 cm⁻¹ wide, and it is associated with this product channel. The angular distribution for this peak, first column in Fig. 5(b), is anisotropic with maxima along the laser polarization axis, $\theta = 0^{\circ}$ and 180° , with [+0.27(3)/+0.08(3)]. This distribution suggests dissociation preferentially from a near-linear geometry and not from the T-shaped geometry of the level prepared. The high-energy 241 cm peak spans a much wider energy region, and it is associated with the Ar + I_2 (β , v_{β} = 0) product channel with possible contributions from dissociation into Ar + I_2 (D', $v_{D'} = 3-5$) products. Its angular distribution is also anisotropic but with maxima at ~45° and ~135° and [+0.23(5)/-0.24(6)].

The angular distributions of the peaks measured when exciting the T-shaped level with two quanta of I_2 vibrational excitation, the $(0,\,0)_2$ level, are similar to those of the $(0,\,0)_1$ level (Fig. S9 in the supplementary material). The lowest energy peak in this KER distribution, at ${\sim}64$ cm $^{-1}$, is tentatively associated with the $\Delta v=-1,\,Ar+I_2$ (D, $v_D=1$) channel. The angular distribution for this peak has maxima at $\theta=0^\circ$ and $180^\circ,\,[+0.20(3)/+0.28(4)].$ The strongest peak in this distribution is at 198 cm $^{-1}$, and it overlaps multiple product channels, including those with the $\Delta v=-2,\,Ar+I_2$ (D, $v_D=0$) channel as well as the $Ar+I_2$ ($\beta,\,v_\beta=1,\,2$) channels. The angular distribution for this peak is considered isotropic, [+0.05(2)/-0.05(2)]. There are no maxima observed in the angular distributions at $\theta=90^\circ$ for excitation of the T-shaped $(0,\,0)_0,\,(0,\,0)_1,\,$ and $(0,\,0)_2$ levels. This contrasts the expectations for the prompt dissociation of $Ar\cdots I_2$ complexes with rigid T-shaped geometries.

Levels with intermolecular vibrational excitation. The $(0, 1)_0$ level, with one quantum of intermolecular stretching excitation, is \sim 33 cm⁻¹ to higher energy than the (0, 0)₀ level, and it is also localized in the T-shaped well within the Ar + I_2 (E, v_E = 0) PES. For this level, the $\Delta v = 0$, Ar + I₂ (D, $v_D = 0$) product channel is energetically open, and there are weak counts in the KER distribution near 4.4 cm⁻¹ associated with it. The angular distribution for this signal, second column in Fig. 5(a), is anisotropic with a distinct maximum at 90°, and the fit yielded anisotropy parameters of [-0.50(1)/-0.15(1)]. This distribution is qualitatively consistent with the prompt dissociation of a complex with a T-shaped geometry. A prominent peak in the KER distribution for the (0, 1)₀ level, centered at ~199 cm⁻¹, is associated with the $\Delta v = 0$, Ar + I₂ $(\beta, v_{\beta} = 0)$ product channel, although there could be contributions from Ar + I_2 (D', $v_{D'} = 0-4$) products since there is a broad tail in the KER distribution extending to higher energies. The angular distribution of this 199 cm⁻¹ peak is anisotropic with weak maxima at $\theta = 0^{\circ}$ and 180°. Similar data could not be collected for excitation to the $(0, 1)_1$ or $(0, 1)_2$ levels due to spectral congestion.

The angular distributions for most of the peaks in the KER distributions for excitation to the $(0, 2)_0$, $(2, 0)_0$, and $(0, 3)_0$ levels with two quanta of stretching, two quanta of bending, and three quanta of stretching excitation, Fig. 5(a), are either anisotropic with maxima at $\theta = 0^{\circ}$ and 180° or isotropic. The continuum tails in the KER distributions for the $(0, 2)_0$ and $(0, 3)_0$ levels suggest that there may be contributions in the peaks and angular distributions from the Ar + I_2 $(D', v_{D'})$ product channels. The $(0, 2)_0$, $(2, 0)_0$, and $(0, 3)_0$ levels with two quanta of stretching, two quanta of bending, and three quanta of stretching excitation, respectively, lie ~63, ~68, and ~91 cm⁻¹ to higher energies than the $(0, 0)_0$ level. Based on the depth of the Ar + I2 (E, vE) PES and the harmonic nature of the intermolecular stretching and bending spectral progression, these levels are localized within the T-shaped well region of the PES. Yet, none of these peaks were measured when exciting these levels have a maximum at $\theta = 90^{\circ}$, which is expected for the dissociation from a T-shaped

The angular distributions for excitation of the $(0, 2)_1$, $(2, 0)_1$, and (0, 3)₁ levels with one quantum of I₂ vibrational excitation are noticeably different than those measured for these same intermolecular levels with no I2 vibrational excitation. The angular distribution of the 33 cm⁻¹ peak in the KER distribution recorded for the $(0, 2)_1$ level, Fig. 5(b), is anisotropic with weak maxima at $\theta = 0^{\circ}$ and 180°. The 248 cm⁻¹ peak in this distribution, however, is isotropic. The two lower-energy peaks in the KER distribution measured for excitation of the $(2, 0)_1$ level and the peak at 59 cm⁻¹ in the distribution for the $(0, 3)_1$ level are anisotropic, each with a distinct maximum at 90°. Thus, even though the $(2, 0)_1$ level is just ~5 cm⁻¹ above the (0, 2)₁ level, the lowest-energy peaks in their KER distributions associated with Ar + I_2 (D, $v_D = 1$) products have starkly different angular distributions. In contrast, the angular distributions for all three peaks in the KER distributions measured for excitation of the $(2, 0)_0$ and $(0, 2)_0$ levels are nearly identical, as mentioned

The anisotropy present in most of the I2 product images indicate the lifetimes of the (n_b, n_s)_{vE} levels prepared, and the dissociation dynamics occur on shorter timescales than the rotational periods of those levels, 300-400 ps.⁴¹ The broadening of the rotational lines present in the two-color, two-photon LIF spectra could also be used to estimate lower limits of the lifetimes of the levels prepared. Attempts were made to fit the rotational contours of several of the features (Fig. S10 in the supplementary material), but statistically relevant fits could not be achieved. Despite this, the attempted fits of the rotational contour of the $(0, 0)_0$ level consistently yielded rotational linewidths just larger than the laser bandwidth, ~0.04 vs ~0.03 cm⁻¹, suggesting a lifetime of ~130 ps or longer. The larger breadths of the rotational lines in the other contours that we attempted to fit, the $(2, 0)_0$, $(0, 4)_0$, $(2, 0)_2$, $(0, 2)_3$, and $(2, 0)_3$ levels, indicate that the complexes in those levels have lifetimes on the order of tens of picoseconds. These values should not be taken quantitatively but instead suggest that the dissociation and dynamics likely occur faster than the rotation of the $(n_b, n_s)_{vE}$ levels.

The highly varying anisotropy results strongly suggest that the dissociation dynamics are not dominated by the intermolecular vibrational excitation prepared within the $(n_b,\,n_s)_{vE}$ levels with

 $v_E=0-2$. Instead, the anisotropies of the I_2 product images appear to be highly dependent on the energy of the level prepared. We propose that this energy dependence arises from energetic resonances and nonadiabatic coupling of the prepared $(n_b,n_s)_{vE}$ levels with dissociative levels energetically above the asymptotes associated with the ion-pair states identified in the I_2 product KER distributions.

IV. DISCUSSION

Transitions to 21 different intermolecular vibrational levels associated with each Ar + I_2 (E, $v_E = 0-2$) PES were recently identified in the I₂ E-B, v_E-23 spectral region, and the binding energies of these potentials were determined to be ~410 cm⁻¹. ^{24,26} Considering that only a subset of the levels lying low in these potentials are optically active due to the preferred C_{2v} symmetry of the complexes, there may be on the order of 100 levels bound within each Ar + I₂ (E, v_E) PES. The large well depth and the relatively small iodine vibrational frequency result in a nesting of the Ar + I2 (E, $v_E = 1-4$) PESs within the Ar + I₂ (E, $v_E = 0$) potential, a high density of Ar···I₂ (E, v_E) intermolecular vibrational levels, and a significant likelihood for levels in the different potentials energetically overlapping each other. The coupling of the levels within the different potentials could result in IVR followed by dissociation into Ar + I₂ (E, v) products, where the product iodine has less vibrational excitation than in the initially prepare level, v < v_E. The PESs and intermolecular vibrational levels of the other ion-pair states in this energy region, specifically the Ar + I_2 (D, v_D), Ar + I_2 (β , v_{β}), and Ar + I₂ (D', v_{D'}) PESs, likely have similar well depths and numbers of bound levels as those in the Ar + I2 (E, vE) PESs. The nonadiabatic coupling of the $(n_b, n_s)_{vE}$ intermolecular vibrational levels with those in the other ion-pair state potentials could give rise to a variety of dynamic interactions, including VP, IVR, and nonadiabatic electronic coupling.

The dynamics of Ar \cdots I₂ complexes prepared in intermolecular vibrational levels within the higher-energy $Ar + I_2$ (E, $v_E = 2-5$) PESs were investigated by Baturo et al. 25,26 In that work, they recorded dispersed fluorescence spectra of the I2 dissociation products and simulated the spectra to determine the contributions from the vibrational products in the I_2 β -A, D-X, and D'-A' spectral regions.² The largest fraction of products were found to be in the I_2 (β , v_{β}) states with partial intensities of the I_2 β -A contributions to the total emission spectra measured to be 78%, 68%, and 38% for excitation to the $(0, 0)_2$, $(0, 1)_2$, and $(0, 1)_5$ levels, respectively.^{25,26} The emission spectrum collected with excitation of the $(0, 1)_2$ level at a total excitation of 41418.5 cm⁻¹ contained contributions from all of the energetically accessible iodine vibrational states in all three ion-pair states, I_2 (β , $v_{\beta} = 0-3$), I_2 (D, $v_D = 0-2$), and I_2 (D', $v_{D'} = 0-8$), with a general trend of the population increasing with product vibrational excitation. ²⁵ A similar trend of increasing I_2 (β , v_{β}) population with higher ν_{β} vibrational excitation was observed when exciting the rigidly T-shaped (0, 0)₂ level.^{25,26} The authors concluded that the $(n_b, n_s)_{vE}$ levels with $v_E = 2-5$ dissociate via a two-step process, non-adiabatic coupling to intermolecular vibrational levels within the other ion-pair state potentials followed by IVR and subsequent dissociation.2

The dissociation of the $(0, 0)_2$ level was the highest-energy level investigated in the VMI experiments presented herein. The I_2 product KER distribution, plotted in Fig. S4 in the supplementary

material, is broad with a weak local maximum associated with I_2 (D, $v_D=1$) or I_2 ($\beta,v_\beta=3$) products, a strong peak attributed to I_2 (D, $v_D=0$) or I_2 ($\beta,v_\beta=1,2$) products, a weak peak associated with the Ar + I_2 ($\beta,v_\beta=0,1$) channels, and a weak tail that must be from Ar + I_2 (D', $v_{D'}=0{\text -}3$) products. Thus, products spanning a range of vibrational levels in all three ion-pair states were identified, which is consistent with the results of Baturo $\it et al.^{25,26}$ Unfortunately, populations in the specific vibrational states could not be quantified in the VMI experiments.

The VMI experiments presented herein primarily focused on the dissociation of low-lying levels bound within the Ar + I $_2$ (E, $v_E=0,\ 1)$ PESs, where the possibility of IVR to other $(n_b,\ n_s)_{vE}$ levels is minimized or not energetically open. The energies of the intermolecular levels spectroscopically identified in the Ar + I $_2$ (E, $v_E=0)$ PES 24 relative to the lower-lying Ar + I $_2$ (D,v $_D=0$ -4) and Ar + I $_2$ (β ,v $_\beta=0$ -5) potentials are schematically shown in Figs. 6(a) and

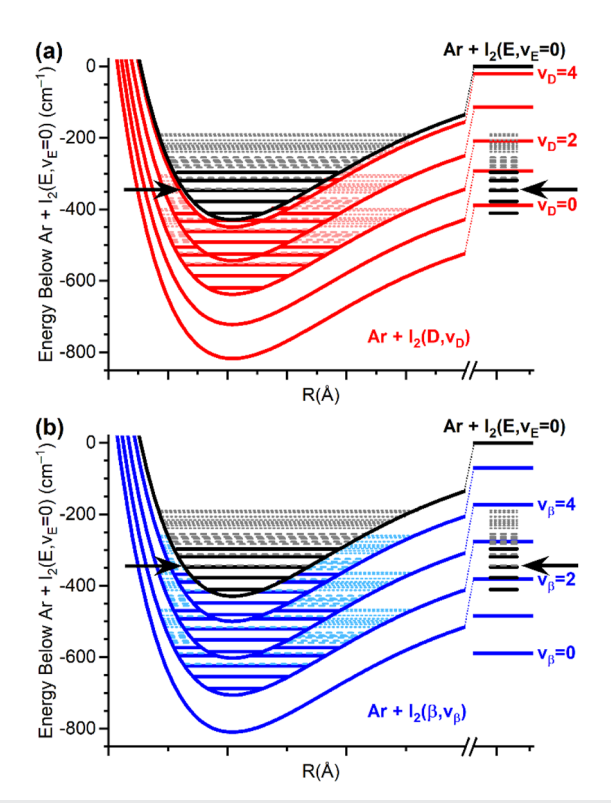


FIG. 6. Schematic of the Ar + I_2 (E, $v_E=0$) (black) potential energy curve, which is nested within the (a) Ar + I_2 (D, $v_D=0$ –4) and (b) Ar + I_2 (β , $v_\beta=0$ –5) potentials. These are Morse potentials for the T-shaped geometry estimated using the stretching frequency and binding energy within the Ar + I_2 (E, $v_E=0$) potential. The potentials are offset by the appropriate I_2 vibronic energies. The lowest-energy T-shaped Ar·· I_2 levels and those with intermolecular stretching excitation are shown as solid lines. Levels with bending excitation are shown as dashed lines, and those lying above the barrier for internal rotation are shown as dotted lines. The energies of the levels within the Ar + I_2 (E, $v_E=0$) potential are also superimposed on the Ar + I_2 (D, $v_D=0$ –4) and Ar + I_2 (β , $v_\beta=0$ –5) asymptotes on the right. The Ar + I_2 (D, $v_D=2$ –4) and Ar + I_2 (β , $v_\beta=0$ –5) potentials and the levels within them are assumed to have the same relative energies as within the Ar + I_2 (E, $v_E=0$) potential to illustrate the expected densities of intermolecular vibrational levels. The energy of the (2, 0)₀ level is indicated with black arrows.

6(b), respectively. The assumption is made for this schematic that the well depths of the Ar + I₂ (D, v_D = 0–4) and Ar + I₂ (β , v_{β} = 0–5) potentials and the levels within them are the same as for the Ar + I₂ (E, v_E) PESs. It is apparent that there is a high density of levels in this energy region because of the nested ion-pair potentials, and it seems likely that at least one (n_b, n_s)_{vD} or (n_b, n_s)_{v β} level could energetically overlap each (n_b, n_s)_{vE} level. In this scenario, there could be simultaneous non-adiabatic coupling and IVR followed by VP into Ar + I₂ (D, v_D) or Ar + I₂ (β , v_{β}) products.

Most of the I₂ product KER distributions recorded for the $(n_b, n_s)_0$ and $(n_b, n_s)_1$ levels and the assignments of the peaks within them indicate that there is a preference for dissociating into $Ar + I_2(D, v_D)$ or $Ar + I_2(\beta, v_\beta)$ products with no change in I_2 vibrational excitation, $v_{\beta} = v_D = v_E$, when these channels are energetically accessible, regardless of the quanta of intermolecular bending and stretching excitation within the prepared level. This trend for forming products with the same I2 vibrational excitation indicates that IVR from the I₂ moiety to the intermolecular vibrational modes does not occur for these levels. Consider, for instance, the dissociation of the $(2, 0)_0$ level, the dashed line indicated with the black arrows in Fig. 6. The $(2, 0)_0$ level could be resonant with low-lying stretching or bending levels in the $Ar + I_2$ (D, $v_D = 4$) potential or highly delocalized levels lying above the barrier to internal rotation within the $Ar + I_2$ (D, $v_D = 1-3$) potentials as indicated in Fig. 6(a). Dissociation through these levels is unlikely considering the I2 vibrational excitation that would have to be gained to populate the Ar \cdots I₂ (D, $v_D = 1-3$) intermolecular levels and then would have to be lost when dissociating into the Ar + I_2 (D, $v_D = 0$) products. The scenario is similar for forming the Ar + I_2 (β , v_{β} = 0) products, Fig. 6(b). The (2, 0)₀ level could be resonant and couple with levels having stretching and bending excitation within the Ar + I_2 (β , v_{β} = 5) potential or delocalized levels within the Ar + I_2 (β , v_β = 3, 4) potentials, but the I2 vibrational excitation within these levels would then have to be redistributed to form the Ar + I_2 (β , v_{β} = 0) products. Instead, we conclude that the initially prepared (n_b, n_s)_{vE} levels dissociate into the $\Delta v = 0$ products via non-adiabatic coupling to the continuum of states lying above the Ar + I_2 (D, $v_D = v_E$) or Ar + I_2 (β , $v_{\beta} = v_{E}$) dissociation limits. Metastable levels above each of these product asymptotes may be involved in this non-adiabatic

As explained in Sec. III B, the prompt dissociation of $Ar \cdots I_2$ complexes with T-shaped geometries would be expected to dissociate into fragments preferentially along an angle of $\theta=90^\circ$ relative to the laser polarization axis for levels accessed with parallel transitions, such as the two-photon excitation in the I_2 B-X and I_2 E-B regions implemented in these VMI experiments. This is what was observed for a small number of the product channels, including the 4 cm⁻¹ signal for the $(0, 1)_0$ level, the 19 cm⁻¹ peak for the $(2, 0)_1$ level, and the 59 cm⁻¹ peak for the $(0, 3)_1$ level. Most of the product angular distributions that are anisotropic, however, have maxima at $\theta=0^\circ$ and 180° . For instance, the lowest-energy peak for the $(0, 2)_0$ level and all three peaks for the $(2, 0)_0$ level each have maxima at $\theta=0^\circ$ and 180° . These levels are localized in the T-shaped well of the Ar + I_2 (E, $v_E=0$) PES and should not sample the linear geometry.

The I_2 product angular distributions measured in similar VMI experiments probing the dissociation of $Ar \cdots I_2$ complexes prepared in levels bound within the $Ar + I_2$ (B, v_B) PESs also contained some

product channels with maxima at $\theta=90^\circ$ and others at $\theta=0^\circ$ and $180^\circ.^7$ The prominent dissociation mechanism for those levels was determined to be IVR followed by VP forming I_2 (B, v_B) products with less vibrational excitation than in the initially excited complex, ranging from $\Delta v=-3$ to $\Delta v=-7$. It was concluded that the dissociation pathway for products with angular distributions with maxima at $\theta=90^\circ$ sampled intermediate levels with T-shaped geometries just prior to VP. Pathways that sampled bending or delocalized internal rotor levels resulted in either isotropic angular distributions or those with maxima at $\theta=0^\circ$ and $180^\circ.$

As stated above, the preferred product channels indicate that a dominant dissociation mechanism of the $(n_b,\,n_s)_{vE}$ levels is through a non-adiabatic coupling with the continuum of states lying above the Ar + I₂ (D, v_D) and Ar + I₂ (β , v_{β}) asymptotes, where $v_E = v_D = v_{\beta}$. Considering the product anisotropy data, we expand on this mechanism by proposing that the nonadiabatic coupling between these levels alters the transition dipole so that it is no longer along the I-I bond axis. This would shift the preferred angular distributions away from $\theta = 90^{\circ}$, even for the dissociation for T-shaped geometries. It is also likely that the significant well depth, 400 cm⁻¹, and the angular anisotropies of the Ar + I_2 (D, v_D) and Ar + I_2 (β , v_{β}) PESs influence the trajectories of the separating Ar and I2 fragments as they traverse just above the lower-energy T-shaped wells associated with the products. As indicated in Fig. 6, the $(2, 0)_0$ level is only ~45 cm⁻¹ above the Ar + I_2 (D, v_D = 0) dissociation limit, and it is ~245 cm⁻¹ above the Ar + I_2 (β , v_{β} = 0) asymptote. The interactions experienced when forming the Ar + I_2 (D', $v_{D'}$) product channels could be even more complicated if these PESs have minima in the linear geometry, as was predicted by Shcherbul' et al.²⁷

Stephenson and co-workers investigated the collision-induced nonadiabatic interactions of I_2 (E, $v_E = 0-2$) states with those in the other first-tier ion-pair states by recording and fitting the product emission spectra. 29,42,43 The full-collision studies of Ar atoms with I_2 (E, $v_E = 0-2$) molecules revealed that there is nonadiabatic coupling of the initially prepared states with the I_2 (β , v_{β}), I_2 (D, v_{D}), and I_2 (D', $v_{D'}$) ion-pair states, with transfer into the I_2 (β , v_{β}) states being slightly preferred. 42,43 The vibrational product-state distribution within each of the product channels is fairly broad with a local maximum at or near the state conserving I₂ vibrational excitation, $\Delta v = 0$. These results were interpreted as the dynamics being dictated by a competition between the Franck-Condon factors associated with the initial and final I2 vibrational states and the minimizing of the fragment KER in accord with the Energy-gap Law.^{29,41,42} The vibrational distribution in the I₂ (D') state formed when exciting the I_2 (E, $v_E = 1$) level does not follow this trend; the calculated Franck-Condon factors peak at $v_{D'} = 1$ and 2, but the measured product-state distribution is broad, spanning $v_{D'} = 0-6$ with a maximum at $v_{D'} = 4$. When exciting the I_2 (E, $v_E = 2$) level, the vibrational distributions of the products are broad for the β , D, and D' states, and there is less agreement between the distributions and the corresponding Franck-Condon factors. 29,42,43

Two primary nonadiabatic mechanisms were identified in these full-collision events, a <u>long-range</u>, <u>approach-induced</u> interaction that dominates for collisions with molecules and a <u>short-range</u>, <u>collision-induced</u> interaction that is prominent for collisions with rare gas atoms. ^{29,44–46} These mechanisms are governed by different selection rules and yield contrasting product-state distributions.

Calculations utilizing the IDIM PT1 model indicated a propensity for coupling between states with opposite inversion parity, Ar + I_2 (E $^3\Pi_{0g}^{-+}$) \rightarrow Ar + I_2 (D 0_u^+), during the collision. ²⁹ It was further proposed that after the collision, there are secondary non-adiabatic interactions that turn on as the Ar and I₂ (D, v_D) separate, and these convert the I₂ (D, v_D) intermediates into I₂ (β, v_{β}) or I_2 (D', $v_{D'}$) products.²⁹ The collision-induced coupling yields broader vibrational and rotational product-state distributions than the approach-induced interactions, although there are dependences of the product-state distributions on the specific I2 (E, vE) level initially prepared and the rare gas collision partner.²⁵

In contrast to the distributions obtained in the full-collision experiments, the vibrational distributions measured in these halfcollision VMI experiments are dominated by the $\Delta v = 0$ products for the Ar + I_2 (D, v_D) and Ar + I_2 (β , v_{β}) channels. The larger population of vibrational product states in the room-temperature collision experiments can be partially attributed to the thermal distribution of collision energies and the Ar + I2 (E, vE) collision events occurring from all intermolecular orientations. This is in stark contrast to preparing a bound intermolecular vibrational level at a specific energy with no center-of-mass translational energy and with preferred intermolecular orientations. At the same time, it seems likely that both the long-range, approach-induced and the short-range, collision-induced interactions that contribute to the full-collision dynamics could both contribute to the dissociation dynamics of the $(n_b, n_s)_{vE}$ levels.

The I_2 (D', $v_{D'}$) population distribution measured in the fullcollision studies contrast those measured in the half-collision VMI experiments. The nonadiabatic coupling of I_2 (E, $v_E = 0$) states with I₂ (D', v_{D'}) states induced by collisions with Ar atoms results in the population in the $v_{D^{\prime}}$ = 0–3 channels, with the overall maximum yield for $v_{D'} = 0$ and a minimum for $v_{D'} = 2$ products. Tails associated with Ar + I_2 (D', $v_{D'}$) products were present in the KER distributions measured following excitation to some of the (n_b, n_s)_{vE} levels in the half-collision VMI experiments. The breadths of these tails indicate that a range of products with $v_{D'} = 0-3$ were formed. Even higher vibrational levels could be populated, but these signals would be overlapped by those of the I_2 (D, v_D) and I_2 (β , v_{β}) products. The signals of the I_2 (D', $v_{D'}$) products in the KER distributions decrease monotonically with decreasing $v_{D^{\prime}}$ and do not indicate a preference for forming $\Delta v = 0$ products, as observed for the Ar + I₂ (D, v_D) and Ar + I_2 (β , v_{β}) channels. These contrasting product-state distributions could suggest a dissimilar non-adiabatic coupling mechanism to the Ar + I_2 (D', $v_{D'} = 0$) products, or they may simply be a result of the significantly larger amount of energy available to the $\Delta v = 0$, $Ar + I_2 (D', v_{D'} = 0)$ products in comparison to the $Ar + I_2 (D, v_D)$ and Ar + I_2 (β , v_{β}) products.

V. CONCLUSIONS

Two-color, two-photon excitation was used to access specific $(n_b, n_s)_{vE}$ intermolecular vibrational levels bound in the Ar + I₂ (E, v_E) PESs. VMI was used to detect the I₂ ion-pair dissociation fragments and measure the KER and angular distributions of the I2 fragments. Each (n_b, n_s)_{vE} level was observed to dissociate into multiple $Ar + I_2$ ion-pair channels. Prominent $Ar + I_2$ product channels are the formation of Ar + I_2 (D, v_D) and Ar + I_2 (β , v_β) products with $v_D = v_\beta v_E$ when those channels are energetically open.

Products are also observed in a range of vibrational levels of the Ar + I_2 (D', $v_{D'}$) channel with $v_{D'} = 0-3$ following excitation of several of the $(n_b, n_s)_{vE}$ levels. The kinetic-energy distributions for this channel are broader, spanning numerous vibrational levels, but there is a trend for minimizing the kinetic energies imparted on the products. Ultimately, the yields in the different Ar + I₂ product channels are likely dictated by a combination of the energy-gap law, the Franck-Condon factors of the initially prepared Ar $\cdot \cdot \cdot I_2$ (E, v_E) level with the intermolecular vibrational levels associated with the different product channels, and the dependence of the non-adiabatic coupling on intermolecular orientation.

The ability to prepare energetically discrete intermolecular vibrational levels with specific quanta of intermolecular bending and stretching excitation, $(n_b, n_s)_{vE}$, and measure the products in the energetically open product channels provides new opportunities for developing our understanding of non-adiabatic coupling. There were significant differences in the product-state distributions predicted by theory with those measured in the full-collision experiments, 29,37,42,43 and numerous questions regarding the nonadiabatic coupling of the I2 (E, vE) states with those of the lowerenergy I_2 (D, v_D), I_2 (β , v_β), and I_2 (D', $v_{D'}$) states remained.⁴³ As mentioned by Chandra and Stephenson, 43 the lack of agreement between the theoretical and experimental product-state distributions could be due to an underestimation of the attractive interactions in the PESs of the ion-pair states. The binding energies of the levels bound within the Ar + I_2 (E, $v_E = 0-3$) PESs^{24,26} as well as both intermolecular stretching and bending frequencies for these PESs²⁴ are now accurately known, and they provide important parameters for developing more accurate potentials, which can, in turn, be used to better characterize the non-adiabatic coupling in the ion-pair states of the model $Ar + I_2$ system.

SUPPLEMENTARY MATERIAL

See the supplementary material for additional VMI data, including I₂⁺ images, momentum distributions, and kinetic-energy release distributions. Specific figures and data included are Figs. S1-S10 and Tables SI and SII.

ACKNOWLEDGMENTS

This work was partially supported by the NSF under Grant No. CSDMA-2102241. Acknowledgment is made to the donors of the American Chemical Society Petroleum Research Fund for partial support of this research.

AUTHOR DECLARATIONS

Conflict of Interest

The authors have no conflicts to disclose.

Author Contributions

Camille Makarem: Conceptualization (equal); Data curation (lead); Formal analysis (equal); Investigation (equal); Methodology (equal); Validation (supporting); Visualization (supporting); Writing – original draft (equal). **Richard A. Loomis**: Conceptualization (equal); Data curation (supporting); Formal analysis (equal); Funding acquisition (lead); Investigation (equal); Methodology (equal); Project administration (lead); Resources (lead); Supervision (lead); Validation (lead); Visualization (lead); Writing – original draft (equal); Writing – review & editing (lead).

DATA AVAILABILITY

The data that support the findings of this study are available within the article and its supplementary material.

REFERENCES

- ¹A. Rohrbacher, J. Williams, and K. C Janda, Phys. Chem. Chem. Phys. 1, 5263 (1999).
- ² A. Rohrbacher, N. Halberstadt, and K. C. Janda, Annu. Rev. Phys. Chem. **51**, 405 (2000).
- ³A. Buchachenko, N. Halberstadt, B. Lepetit, and O. Roncero, Int. Rev. Phys. Chem. **22**, 153 (2003).
- ⁴A. A. Buchachenko, O. Roncero, and N. F. Stepanov, Russ. J. Phys. Chem. **74**, S193 (2000).
- ⁵G. Kubiak, P. S. H. Fitch, L. Wharton, and D. H. Levy, J. Chem. Phys. 68, 4477 (1978).
- ⁶C. Makarem and R. A. Loomis, Chem. Phys. Lett. **651**, 119 (2016).
- ⁷C. Makarem, J. Wei, R. A. Loomis, and J. P. Darr, Phys. Chem. Chem. Phys. 23, 26108 (2021).
- ⁸J. A. Blazy, B. M. DeKoven, T. D. Russell, and D. H. Levy, J. Chem. Phys. **72**, 2439 (1980).
- ⁹O. Roncero, B. Lepetit, J. A. Beswick, N. Halberstadt, and A. A. Buchachenko, J. Chem. Phys. 115, 6961 (2001).
- ¹⁰ M. L. Burke and W. Klemperer, J. Chem. Phys. **98**, 6642 (1993).
- ¹¹ M. L. Burke and W. Klemperer, J. Chem. Phys. **98**, 1797 (1993).
- ¹²B. Lepetit, O. Roncero, A. A. Buchachenko, and N. Halberstadt, J. Chem. Phys. 116, 8367 (2002).
- ¹³O. Roncero, A. A. Buchachenko, and B. Lepetit, J. Chem. Phys. **122**, 034303 (2005).
- ¹⁴O. Roncero and S. K. Gray, J. Chem. Phys. **104**, 4999 (1996).
- ¹⁵S. K. Gray and O. Roncero, J. Phys. Chem. **99**, 2512 (1995).
- ¹⁶S. K. Gray, Chem. Phys. Lett. 197, 86 (1992).
- ¹⁷O. Roncero, N. Halberstadt, and J. A. Beswick, J. Chem. Phys. **104**, 7554 (1996).
- ¹⁸ A. Bastida, J. Zuniga, A. Requena, N. Halberstadt, and J. A. Beswick, Chem. Phys. 240, 229 (1999).
- ¹⁹E. M. Goldfield and S. K. Gray, J. Chem. Soc., Faraday Trans. 93, 909 (1997).
- ²⁰E. M. Goldfield and S. K. Gray, Chem. Phys. Lett. **276**, 1 (1997).

- ²¹ A. E. Stevens Miller, C.-C. Chuang, H. C. Fu, K. J. Higgins, and W. Klemperer, J. Chem. Phys. 111, 7844 (1999).
- ²² N. Zeigler, C. Makarem, J. Wei, and R. A. Loomis, J. Chem. Phys. **152**, 094303 (2020).
- ²³ J. P. Darr, J. J. Glennon, and R. A. Loomis, J. Chem. Phys. **122**, 131101 (2005).
- ²⁴C. Makarem and R. A. Loomis, Chem. Phys. Lett. 826, 140642 (2023).
- ²⁵V. V. Baturo, I. N. Cherepanov, S. S. Lukashov, S. A. Poretsky, and A. M. Pravilov, Chem. Phys. Lett. 647, 161 (2016).
- ²⁶ V. V. Baturo, S. S. Lukashov, S. A. Poretsky, and A. M. Pravilov, Eur. Phys. J. D 71, 227 (2017).
- ²⁷T. V. Shcherbul', A. V. Zaitsevskii, A. A. Buchachenko, and N. F. Stepanov, Russ. J. Phys. Chem. 77, 511 (2003).
- ²⁸T. V. Shcherbul', Y. V. Suleimanov, and A. A. Buchachenko, Russ. J. Phys. Chem. **80**, 1957 (2006).
- ²⁹T. V. Tscherbul, A. A. Buchachenko, M. E. Akopyan, S. A. Poretsky, A. M. Pravilov, and T. A. Stephenson, Phys. Chem. Chem. Phys. 6, 3201 (2004).
- ³⁰ J. Wei, C. Makarem, A. L. Reinitz, J. P. Darr, and R. A. Loomis, Chem. Phys. 399, 172 (2012).
- ³¹ Y. Zhang, K. Vidma, D. H. Parker, and R. A. Loomis, J. Chem. Phys. 130, 104302 (2009).
- 32 V. Dribinski, A. B. Potter, I. Fedorov, and H. Reisler, J. Chem. Phys. **121**, 12353 (2004)
- ³³V. Dribinski, A. Ossadtchi, V. A. Mandelshtam, and H. Reisler, Rev. Sci. Instrum. 73, 2634 (2002).
- ³⁴M. L. Nowlin and M. C. Heaven, Chem. Phys. Lett. **239**, 1 (1995).
- ³⁵J. P. Perrot, M. Broyer, J. Chevaleyre, and B. Femelat, J. Mol. Spectrosc. 98, 161 (1983).
- ³⁶ X. Zheng, S. Fei, M. C. Heaven, and J. Tellinghuisen, J. Chem. Phys. **96**, 4877 (1992).
- 37 M. E. Akopyan, A. A. Buchachenko, S. S. Lukashov, S. A. Poretsky, A. M. Pravilov, Y. V. Suleimanov, A. S. Torgashkova, and T. V. Tscherbul, Chem. Phys. Lett. 436, 1 (2007)
- ³⁸ J.-K. Wang, Q. Liu, and A. H. Zewail, J. Phys. Chem. **99**, 11309 (1995).
- ³⁹R. N. Zare, Mol. Photochem. **4**, 1 (1972).
- ⁴⁰ K. m. Chen and E. S. Yeung, J. Chem. Phys. **72**, 4723 (1980).
- ⁴¹J. C. D. Brand, A. K. Kalukar, and A. B. Yamashita, Opt. Commun. **39**, 235 (1981).
- ⁴²C. J. Fecko, M. A. Freedman, and T. A. Stephenson, J. Chem. Phys. 116, 1361 (2002)
- ⁴³P. P. Chandra and T. A. Stephenson, J. Chem. Phys. **121**, 2985 (2004).
- ⁴⁴T. V. Tscherbul and A. A. Buchachenko, J. Phys. B: At., Mol. Opt. Phys. **37**, 1605 (2004).
- ⁴⁵ M. E. Akopyan, V. V. Baturo, S. S. Lukashov, S. A. Poretsky, and A. M. Pravilov, Chem. Phys. **462**, 3 (2015).
- ⁴⁶S. Lukashov, A. Petrov, and A. Pravilov, *The Iodine Molecule: Insights into Intra*and Intermolecular Perturbation in Diatomic Molecules (Springer, Switzerland, 2018)